PHYSICAL REVIEW B **93**, 155116 (2016)

All-electron mixed basis *GW* calculations of TiO_2 and ZnO crystals

Ming Zhang,[1] Shota Ono,[1] Naoki Nagatsuka,[1,2] and Kaoru Ohno[1,*]
[1]*Department of Physics, Graduate School of Engineering, Yokohama National University, 79-5 Tokiwadai, Hodogaya, Yokohama 240-8501, Japan*
[2]*Institute of Industrial Science, The University of Tokyo, 4-6-1 Komaba, Meguro, Tokyo 153-8505, Japan*

(Received 21 September 2015; revised manuscript received 2 February 2016; published 8 April 2016)

In transition metal oxide systems, there exists a serious discrepancy between the theoretical quasiparticle energies and the experimental photoemission energies. To improve the accuracy of electronic structure calculations for these systems, we use the all-electron mixed basis *GW* method, in which single-particle wave functions are accurately described by the linear combinations of plane waves and atomic orbitals. We adopt the full ω integration to evaluate the correlation part of the self-energy and compare the results with those obtained by plasmon pole models. We present the quasiparticle energies and band gap of titanium dioxide (TiO_2) and zinc oxide (ZnO) within the one-shot *GW* approximation. The results are in reasonable agreement with experimental data in the case of TiO_2 but underestimated by about 0.6–1.4 eV from experimental data in the case of ZnO, although our results are comparable to previous one-shot *GW* calculations. We also explain a new approach to perform ω integration very efficiently and accurately.

DOI: 10.1103/PhysRevB.93.155116

I. INTRODUCTION

Because of their unique band structure properties, the transition metal oxides have wide applications in electronics and optoelectronics. The unusual properties are due to the unique nature of the outer *d* electrons, which enlarges local electron correlations.

Titanium dioxide (TiO_2) is one of the most investigated transition metal oxides, useful for a wide variety of photocatalytic, thermoelectric, solar cell, biosensing, and gas sensing applications. It exhibits several phases. The experimental band gap of anatase TiO_2 is known to be 3.2 eV [1] or 3.4 eV [2], while that of rutile TiO_2 has a quite large degree of uncertainty: 3.3 ± 0.5 eV [3], 3.6 ± 0.2 eV [4], and 4.0 eV [5].

Zinc oxide (ZnO) is a II–VI compound transition metal oxide having wide electronic and optoelectronic applications, such as in transparent electrodes, light-emitting diodes, and solar cells. ZnO crystallizes in two main forms, hexagonal wurtzite and cubic zincblende. The experimental band gap of hexagonal wurtzite ZnO is about 3.6 eV [6,7] or 3.437 eV [8]. The band gap of cubic zincblende ZnO is 3.44 eV at low temperatures [9,10] and 3.37 eV at room temperature [10]. All these data were obtained by photoemission spectroscopy measurements.

Although TiO_2 and ZnO have been studied for many decades, it is still challenging to theoretically reproduce their electronic structures correctly. Transition metal oxides have open *d*-electron shells, where electrons occupy localized orbitals. Electrons experience strong Coulombic repulsion because of their spatial confinement in those orbitals. Most calculations of the electronic structure of transition metal oxides have been done within the density-functional theory (DFT) [11]. However, the Kohn-Sham (KS) eigenvalues underestimate the band gap compared with the experimental (inverse) photoemission data, due to the well-known deficiency that the KS eigenvalues are not the quasiparticle (QP) energies. In order to discuss the physical band gap, the QP energies are needed [12]. The QP picture is based on the many-body Green's function theory. The *GW* approximation [12–15] is the most commonly used QP Green's function method on the basis of many-body perturbation theory (MBPT) [13].

The one-shot *GW* approximation solves the QP equation within the first-order approximation for the difference between the self-energy and the LDA potential. It has been successfully applied for a broad class of materials ranging from bulk insulators to semiconductors [14–17]. Some *GW* calculations of TiO_2 and ZnO have been reported (see also Table I): For anatase TiO_2, Kang and Hybertsen [18] reported an X-Γ indirect band gap of 3.56 eV in a one-shot *GW* calculation. Patrick and Giustino [19] obtained a 3.3-eV band gap starting from DFT + U. For rutile TiO_2, the band gap values of 3.34 eV [18], 4.8 eV [20], and 3.59 eV [21] were reported by the one-shot *GW* method. The use of the generalized plasmon pole (GPP) model [15] overestimates the band gap at 4.48 eV [18]. We have also performed a one-shot *GW* calculation for rutile TiO_2 with and without Nb impurities [22] (hereafter we refer to Ref. [22] as "I") and obtained 3.30 eV for the band gap for pure rutile TiO_2. Schilfgaarde *et al.* [23,24] performed a full-potential LMTO-based self-consistent *GW* calculation and obtained 3.78 eV. Lany [25] used the self-consistent *GW* calculation with a fixed GGA + U wave function and obtained 4.48 eV. He also obtained TDDFT-based local-field-corrected values of 3.11 and 3.4 eV by introducing the empirical *d*-orbital on-site energy. For wurtzite ZnO, band-gap values of 2.44 eV [26] and 4.23 eV [27] were reported earlier using the one-shot *GW* method and the model *GW* method, respectively. More recently, Shih *et al.* [28] claimed that the conventional one-shot *GW* method can give a band gap that is very close to the experimental value, if one uses enough high-cutoff energies, many empty states, and the GPP model. However, Friedrich *et al.* [29,30] and Stankovski *et al.* [31] showed that this agreement is an artifact of using the GPP model; see also Ref. [32]. In particular, Friedrich *et al.* [29,30], in a careful comparison with previous all-electron *GW* results concerning the number of levels and basis set, obtained a one-shot *GW* band gap of 2.83 eV for wurtzite ZnO. Their results were still far smaller than the experimental band gap. Thus, there

---

[*] ohno@ynu.ac.jp

TABLE I. Band gaps of TiO_2 and ZnO calculated by the LDA and *GW* methods (in eV). For "previous *GW*" results, values without an explanation in parentheses denote the one-shot *GW* method, while sc*GW* denotes the self-consistent *GW* method, and so on. GPP, one-shot *GW* method using the GPP model; vLH, plasmon pole model of von der Linden–Horsch [39]; ω'-int., ω' integration.

	LDA	Present *GW*			Previous *GW*	Expt.
		GPP	vLH	ω'-int.		
Anatase TiO_2	1.70	5.73	4.46	3.44	3.56,[a] 3.3(*GW* with DFT + U)[b]	3.4[c]
Rutile TiO_2	1.76	4.0	3.3	3.30	4.48(GPP),[a] 3.34,[a] 4.8,[d] 3.59,[e] 3.30,[f] 3.78(sc*GW*),[g] 4.48(sc*GW* with GGA + U)[h]	3.3 ± 0.5[i]
Wurtzite ZnO	1.10	4.54	3.91	2.82	2.44,[j] 4.23(model *GW*),[k] 3.4(GPP),[l] 3.6(GPP/LDA + U),[l] 2.83,[m] 2.352,[n] 2.56,[o] 3.88($GW\Gamma^1$)[p]	3.4[q]
Zincblende ZnO	1.07	3.50	2.61	2.01	2.12,[r] 2.54(GW_0),[r] 3.0(GW_0),[s] 3.2(sc*GW*)[r],[s]	3.4[t]

[a] From Ref. [18].
[b] From Ref. [19].
[c] From Ref. [2].
[d] From Ref. [20].
[e] From Ref. [21].
[f] From Ref. [22].
[g] From Refs. [23] and [24].
[h] From Ref. [25].
[i] From Ref. [3].
[j] From Ref. [26].
[k] From Ref. [27].
[l] From Ref. [28].
[m] From Ref. [30].
[n] From Ref. [31].
[o] From Ref. [32].
[p] From Ref. [33].
[q] From Ref. [8].
[r] From Ref. [34].
[s] From Ref. [35].
[t] From Ref. [10].

has been debate over this GW band-gap issue. To improve the calculation method, Crüneis *et al.* [33] adopted the $GW\Gamma^1$ method, i.e., partially self-consistent $GW^{\text{TC-TC}}$@HSE + single-shot vertex correction for the self-energy and obtained a 3.88-eV band gap. This is, however, about 0.44 eV larger than the experimental value [8]. For zincblende ZnO, Shishkin and Kresse [34,35] reported a 2.12-eV band gap in the one-shot *GW* method, 2.54 and 3.0 eV in the GW_0 method, 3.2 eV in the *GW* method, and 3.2 eV for the self-consistent *GW* with (*e-h*) attractive electron-hole interaction (TC-TC approximation in W). In these calculations of ZnO, however, the results do not satisfactorily agree with the experimental data even when self-consistent *GW* calculations and the $GW\Gamma^1$ method were performed. This means that the self-consistent *GW* method does not improve the one-shot *GW* results in the sense that the former does not satisfy the Ward-Takahashi identity, i.e., the gauge invariance or the local charge continuity [36].

However, even within the same method, the values of the *GW* band gap are very scattered. There are two main reasons. (i) Local fields [37,38] play an important role in the calculation of the dielectric function $\epsilon(\omega)$ and can cause a significant reduction in the dielectric function. The GPP model, introduced by Hybertsen and Louie [14,15], treats local-field effects [the off-diagonal elements of the dielectric matrix $\epsilon_{\mathbf{G},\mathbf{G}'}(\omega)$ for reciprocal lattice vectors $\mathbf{G}$, $\mathbf{G}'$] as a simple function, whose imaginary part is a symmetric delta function for positive and negative ω and real part reproduces its static value in the limit $\omega \to 0$ and the first frequency moment $\omega^2\chi(\mathbf{r},\mathbf{r}';\omega)$ in the limit $\omega \to \infty$ so as to satisfy Johnson's sum rule. This treatment still needs the double summation with respect to $\mathbf{G}$, $\mathbf{G}'$ in the evaluation of the expectation values of the self-energy. von der Linden and Horsch [39] showed that it is possible to convert this double summation into a single summation with respect to the plasmon poles, which is related to the eigenvalue of the dielectric matrix $\epsilon_{\mathbf{G},\mathbf{G}'}(\omega)$ in the limit of $\omega \to 0$. In either way, the QP energies of typical semiconductors have been successfully reproduced to within 0.1 to 0.4 eV. However, when there exists a strong structure in the ω dependence of $\epsilon_{\mathbf{G},\mathbf{G}'}(\omega)$, which cannot be represented by a single plasmon pole, the use of the GPP model or other plasmon pole model is not justified for describing the dynamical dielectric response [18]. In the case of rutile TiO_2, for example, the GPP model leads to too large a band gap ([18]; see also I).

(ii) The one-shot *GW* quasiparticle energy is determined by KS eigenvalues and wave functions. Therefore different pseudopotentials and exchange-correlation functionals may lead to *GW* band-gap differences. The problem in generating good pseudopotentials is related to the fact that the core contribution to the exchange-correlation potential is not simply an additive quantity. Moreover, it is not easy to create efficient pseudopotentials, which require only a small number of plane waves (PWs).

In order to obtain an accurate band gap of $\mathrm{TiO_2}$ and ZnO within the one-shot *GW* approximation, we adopt the all-electron mixed basis *GW* method, in which the single-particle wave functions are accurately described by both PWs and atomic orbitals (AOs). The present approach is capable of describing spatially localized states as well as extended states quite well. We use the standard Perdew-Zunger's exchange-correlation functional [40] and the full ω integration as well as the plasmon pole models to evaluate the correlation part of the self-energy.

The paper is organized as follows: in Sec. II we describe the theory; computational details are described in Sec. III. In Sec. IV we report the results for $\mathrm{TiO_2}$ and ZnO. Section V is devoted to discussion, and finally, in Sec. VI we draw our conclusions.

II. THEORY

The QP energies $\varepsilon_{n\mathbf{k}}^{\mathrm{QP}}$ and wave functions $\psi_{n\mathbf{k}}$ are obtained by solving the QP equation [12,13],

$$(T+V_{\mathrm{ext}}+V_H)\psi_{n\mathbf{k}}(\mathbf{r})+\int d\mathbf{r}'\,\Sigma_{xc}\big(\mathbf{r},\mathbf{r}';\varepsilon_{n\mathbf{k}}^{\mathrm{QP}}\big)\psi_{n\mathbf{k}}(\mathbf{r}')=\varepsilon_{n\mathbf{k}}^{\mathrm{QP}}\psi_{n\mathbf{k}}(\mathbf{r}), \tag{1}$$

where T, V_{ext}, V_H, and Σ_{xc} are the kinetic energy operator, the nuclear Coulomb potential, the Hartree potential, and the exchange-correlation part of the nonlocal, energy-dependent self-energy, respectively. For comparison, the KS equation is given by

$$(T+V_{\mathrm{ext}}+V_H)\psi_{n\mathbf{k}}^{\mathrm{LDA}}(\mathbf{r})+V_{xc}^{\mathrm{LDA}}\psi_{n\mathbf{k}}^{\mathrm{LDA}}(\mathbf{r})=\varepsilon_{n\mathbf{k}}^{\mathrm{LDA}}\psi_{n\mathbf{k}}^{\mathrm{LDA}}(\mathbf{r}), \tag{2}$$

where V_{xc}^{LDA} is the exchange-correlation potential. In the QP equation, the exchange-correlation part of the self-energy Σ_{xc} replaces the exchange-correlation potential V_{xc}^{LDA} in the KS equation.

A formally exact way of calculating the self-energy is given by a set of coupled equations, known as Hedin's equations [12,13]. Hedin's equations are a closed set of integrodifferential equations that relate the Green function G, the polarizability P, the Coulomb interaction between electrons v, the dynamically screened Coulomb interaction W, the self-energy (including the Hartree potential) Σ, and the vertex function Γ. In the *GW* approximation, the vertex function Γ is replaced by its zeroth-order approximation, i.e., unity. So the set of Hedin's equations becomes

$$\Sigma(1,2)=iG(1,2)W(1^+,2), \tag{3}$$

$$G(1,2)=G_0(1,2)+\iint d(3)d(4)G_0(1,3)\Sigma(3,4)G(4,2), \tag{4}$$

$$W(1,2)=v(1,2)+\iint d(3)d(4)v(1,3)P(3,4)W(4,2), \tag{5}$$

$$P(1,2)=-iG(1,2)G(2,1), \tag{6}$$

$$G(\mathbf{r},\mathbf{r}';\varepsilon)=\sum_{n\mathbf{k}}\frac{\psi_{n\mathbf{k}}(\mathbf{r})\psi_{n\mathbf{k}}^{*}(\mathbf{r}')}{\varepsilon-\varepsilon_{n\mathbf{k}}^{\mathrm{QP}}-i\delta_{n\mathbf{k}}}, \tag{7}$$

where G_0 is the noninteracting Green function and $\delta_{n\mathbf{k}}$ stands for 0^+ for occupied states and 0^- for empty states. A compressed notation is used in which $1\equiv(\mathbf{r}_1,t_1)$ are space-time coordinates for quasiparticle 1 and $1^+\equiv(\mathbf{r}_1,t_1+0^+)$. For simplicity, we have omitted spin indices.

Using the one-shot *GW* approximation, the quasiparticle equation can be solved within the first-order approximation in $(\Sigma_{xc}^{GW}-V_{xc}^{\mathrm{LDA}})$. The KS wave functions $\psi_{n\mathbf{k}}^{\mathrm{LDA}}$ and the true QP wave functions $\psi_{n\mathbf{k}}(\mathbf{r})$ are usually sufficiently close, so that the first-order estimate of the self-energy correction to the DFT eigenvalues is still efficient [15]. So the *GW* quasiparticle energy $\varepsilon_{n\mathbf{k}}^{\mathrm{QP}}$ is then obtained as

$$\varepsilon_{n\mathbf{k}}^{\mathrm{QP}}=\varepsilon_{n\mathbf{k}}^{\mathrm{LDA}}+Z_{n\mathbf{k}}\big\langle\psi_{n\mathbf{k}}^{\mathrm{LDA}}\big|\,\Sigma_{xc}^{GW}\big(\varepsilon_{n\mathbf{k}}^{\mathrm{LDA}}\big)-V_{xc}^{\mathrm{LDA}}\,\big|\psi_{n\mathbf{k}}^{\mathrm{LDA}}\big\rangle, \tag{8}$$

with the renormalization factor as

$$Z_{n\mathbf{k}}=\left[1-\frac{\partial\Sigma_{xc}^{GW}(\varepsilon)}{\partial\varepsilon}\right]^{-1}_{\varepsilon=\varepsilon_{n\mathbf{k}}^{\mathrm{LDA}}}. \tag{9}$$

The *GW* self-energy can be separated into the exchange part Σ_x and the correlation part Σ_c ($\Sigma_{xc}^{GW}=\Sigma_x+\Sigma_c$). The exchange part is given by

$$\Sigma_x(\mathbf{r},\mathbf{r}')=-\sum_{n\mathbf{k}}^{\mathrm{occ}}\frac{\psi_{n\mathbf{k}}(\mathbf{r})\psi_{n\mathbf{k}}^{*}(\mathbf{r}')}{|\mathbf{r}-\mathbf{r}'|}. \tag{10}$$

The symbol "occ" in the sum means that the summation is taken over the occupied states only. The on-site contribution to the Fock exchange matrix elements composed of four AOs centered at the same nucleus is evaluated analytically (numerically in the radial direction by using a logarithmic mesh) in real space. This treatment guarantees the accuracy of the Fock exchange contribution. On the other hand, the core states are not taken into account in the summation over occupied states in the evaluation of the polarization function and the correlation part of the self-energy. The correlation part of the self-energy, $\Sigma_c(\mathbf{r},\mathbf{r}';\omega)$, is evaluated either by using the plasmon pole models or by using the full ω' integration [41]:

$$\Sigma_c(\mathbf{r},\mathbf{r}';\omega)=\frac{i}{2\pi}\int d\omega' e^{-i\omega 0^+}G(\mathbf{r},\mathbf{r}';\omega-\omega')\times[W(\mathbf{r},\mathbf{r}';\omega')-v(\mathbf{r}-\mathbf{r}')]. \tag{11}$$

In Eq. (11), it is difficult to perform the ω' integral along the real axis, since W and G have a strong structure on this axis. In order to avoid this difficulty, Godby *et al.* [16,17,42,43] restricted the values of ω to small imaginary numbers and changed the contour of the ω' integral from the real axis to the imaginary axis. Then, by analytic continuation, the resulting Taylor series is used to estimate the matrix elements for real values of ω. (There is also a method that does not use analytic continuation by keeping the Hermiticity of W.)

Ishii and Ohno [41,44] suggested that this integration method employed by Godby *et al.* [16,17,42,43] can be extended rather easily to real numbers of ω by slightly modifying the contour. The contour along the real ω' axis from $-\infty$ to $+\infty$ for the integral in Eq. (11) can be replaced by the contour C shown in Fig. 1 when $\omega<0$. Here we further use the symmetry $W(\omega) = W(-\omega)$ to reduce the contour to the positive real and imaginary parts only; see also I. The diagonal matrix element of the correlation part of the self-energy becomes

$$\langle n,\mathbf{k}|\,\Sigma_c(\mathbf{r},\mathbf{r}';\omega)\,|n,\mathbf{k}\rangle = \sum_{n'}\sum_{\mathbf{q}}\sum_{\mathbf{G},\mathbf{G}'}\langle n,\mathbf{k}|e^{i(\mathbf{q}+\mathbf{G})\cdot\mathbf{r}}|n',\mathbf{k}-\mathbf{q}\rangle \times \langle n'\mathbf{k}-\mathbf{q}|e^{-i(\mathbf{q}+\mathbf{G})\cdot\mathbf{r}}|n,\mathbf{k}\rangle \frac{i}{2\pi}\int_{C'} d\omega'[W_{\mathbf{G},\mathbf{G}'}(\mathbf{q},\omega') - (4\pi/\Omega G^2)\delta_{\mathbf{G},\mathbf{G}'}]\left(\frac{1}{\omega+\omega'-\varepsilon_{n\mathbf{k}-\mathbf{q}}-i\delta_{n\mathbf{k}-\mathbf{q}}} + \frac{1}{\omega-\omega'-\varepsilon_{n\mathbf{k}-\mathbf{q}}-i\delta_{n\mathbf{k}-\mathbf{q}}}\right) \tag{12}$$

in the case when we only perform the contour integration along the positive (real and imaginary) parts C' of the contour C shown in Fig. 1. If we use the original contour C, the second term in parentheses of the integrand in Eq. (12) does not appear.

This contour is justified as follows: The important point is that the polarization function

$$P^0(\mathbf{r},\mathbf{r}';\omega') = 2\sum_{n\mathbf{k}}\sum_{n'\mathbf{k}'}\frac{\psi_{n\mathbf{k}}(\mathbf{r})\psi^*_{n'\mathbf{k}'}(\mathbf{r})\psi^*_{n\mathbf{k}}(\mathbf{r}')\psi_{n'\mathbf{k}'}(\mathbf{r}')}{\omega'-\varepsilon_{n\mathbf{k}}+\varepsilon_{n'\mathbf{k}'}-i\delta_{n\mathbf{k}}} \times[f(\varepsilon_{n'\mathbf{k}'})-f(\varepsilon_{n\mathbf{k}})] \tag{13}$$

[2 is the spin duplicity and $f(x)$ is the Fermi distribution function], and therefore $W(\omega')$ also have poles only in the regions [Re$(\omega') > 0$, Im$(\omega') < 0$)] and [Re$(\omega') < 0$, Im$(\omega') > 0$]. There are also poles from the Green's function $G(\omega' + \omega)$ in the regions [Re$(\omega') > -\omega$, Im$(\omega') < 0$] and [Re$(\omega') < -\omega$, Im$(\omega') < 0$] when we set the Fermi energy at 0. Therefore, poles exist in the combined regions [Re$(\omega') > 0$, Im$(\omega') < 0$] and [Re$(\omega') < -\omega$, Im$(\omega') > 0$] for $\omega < 0$. These poles are illustrated as X's in Fig. 1. Therefore, we can bend the contour 90° along the real ω' axis to the axis parallel to the imaginary ω' axis at $\omega' = \pm\omega_1$. Therefore, ω_1 should be set at max(ω), and $-\omega_1$ should be set at min(ω). Since ω is set at $\varepsilon_{n\mathbf{k}}$, the contour on the real axis $(-\omega_1,\omega_1)$ must enclose the whole region where we need to evaluate the QP spectra. But, nevertheless, this deformed contour integration is very simple and can be further simplified onto the positive real axis $(0,\omega_1)$ and positive imaginary axis shifted to $\omega' = \omega_1$, i.e., $(\omega_1,\omega_1 + iA)$, where A is a large positive number. This method of performing ω integration is very efficient and accurate; see also I.

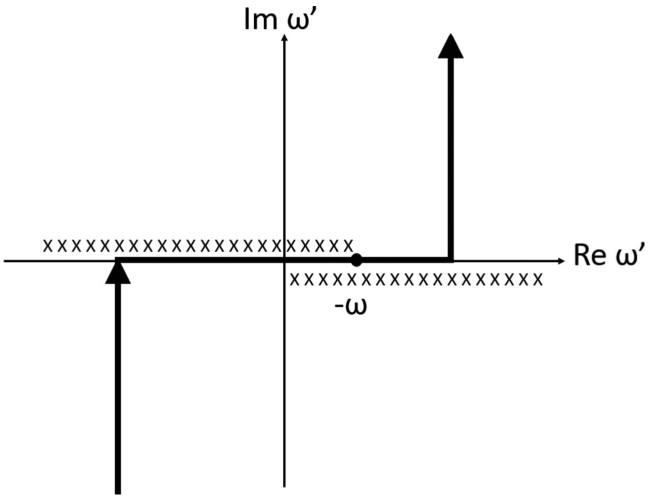

FIG. 1. Contour C of the ω' integration in Eq. (11).

III. COMPUTATIONAL DETAILS

The electronic structures of TiO_2 and ZnO are calculated by the one-shot GW method as in I using the all-electron mixed basis code, TOMBO [45,46]. In order to treat periodic systems as well as isolated systems within an all-electron formalism, we have developed this all-electron mixed basis approach [47–49], where single-electron wave functions are expressed as a linear combination of PWs and AOs, and implemented the GW routine [48,50,51]. The PW basis set can most accurately describe the empty states. In contrast, the AO basis set works better than the PW basis set to describe the electrons in the core region accurately. The all-electron mixed basis approach, using both PWs and AOs as a basis set in a combined way, meets the requirements to describe both spatially extended and localized states:

$$\psi_v(\mathbf{r}) = \frac{1}{\sqrt{\Omega}}\sum_{\mathbf{G}} c_v^{\mathrm{PW}}(\mathbf{G})e^{i\mathbf{G}\cdot\mathbf{r}} + \sum_j\sum_{nlm} c_v^{\mathrm{AO}}(jnlm)\phi^{\mathrm{AO}}_{jnlm}(\mathbf{r}-\mathbf{R}_j). \tag{14}$$

Here, Ω is the volume of the unit cell, $\mathbf{G}$'s are the reciprocal lattice vectors, and c's are the expansion coefficients. In TOMBO code, AOs are numerically confined inside the nonoverlapping atomic spheres by subtracting a parabolic function smoothly connecting with the true AO (the subtracted part as well as the true AO outside the nonoverlapping sphere is well described by PWs), and the radial part is treated using the logarithmic mesh.

The lattice parameters of TiO_2 and ZnO are set as follows: $a = b = 3.78$ Å, $c = 9.50$ Å, $u = 0.208$ for anatase TiO_2 [52]; $a = b = 4.59$ Å, $c = 2.96$ Å, $u = 0.305$ for rutile TiO_2 [53]; $a = b = 3.25$ Å, $c = 5.21$ Å, $u = 0.382$ for wurzite ZnO [54]; and $a = b = c = 4.62$ Å, $u = 0.433$ for zincblende ZnO [55]. The GW calculations using TOMBO require the following settings: The correlation part of the self-energy, Σ_c, is calculated by performing the full ω integration using 201 points at $0.1 + 0.2n$ (eV) and $20.1 + (1 + 2n)i$ (eV) for $n = 0$ and 100 along the positive real axis and then rotated 90° parallel to the positive imaginary axis as in I; see Fig. 1. In this work, we treat $1s^2 2s^2 2p^6 3s^2 3p^6$ as core states for the Ti and Zn atoms (AOs confined within a radius of 0.8 Å) and $1s^2$ for O atoms (AOs confined within a radius of 0.65 Å). The crystal structure, the first Brillouin zone (BZ), and special $\mathbf{k}$ points are shown in Fig. 2 and Fig. 3, respectively, for TiO_2 and ZnO. For

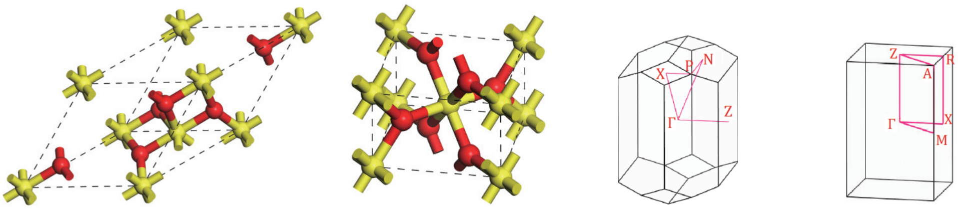

(a)anatase TiO_2 (b)rutile TiO_2 (c)1st BZ of anatase TiO_2 (d)1st BZ of rutile TiO_2

FIG. 2. Crystal structure of (a) anatase TiO_2 and (b) rutileTiO_2; first Brillouin zone (BZ) and special **k** points of (c) anatase TiO_2 and (d) rutile TiO_2. Red atoms, oxygen; yellow atoms, titanium.

anatase TiO_2, the cutoff energies are set at 18.29 Ry for PWs, 73.14 for Fock exchange, and 9.33 Ry for correlation. For LDA calculations, $4 \times 4 \times 4$ **k** points are used. To calculate the polarization function, **k**-point sampling is performed for the $(3 \times 3 \times 3)$ points including the Γ point in the whole BZ. The number of levels used in the summation is 500. The exchange and correlation parts of the self-energy are evaluated by taking four **q**-point (Γ grid) samplings in the irreducible BZ. For rutile TiO_2, wurtzite ZnO, and zincblende ZnO, $5 \times 5 \times 8, 6 \times 6 \times 6$, and $4 \times 4 \times 4$ **k** points are used for LDA calculations, respectively; $3 \times 3 \times 5$ points, $3 \times 3 \times 3$, and $3 \times 3 \times 3$ **k** points including the Γ point are used to calculate the polarization function, respectively. The cutoff energies of PWs, Fock exchange, and correlation are set at 33.58, 170.01, and 13.12 Ry for rutile TiO_2; 205.23, 603.14, and 104.71 Ry for wurtzite ZnO; and 127.54, 510.17, and 127.54 Ry for zincblende ZnO, respectively. These quite high cutoff energies are required to represent fully occupied localized 3*d* orbitals of Zn atoms in the mixed basis representation. Six **q** points and 400 levels are used in rutile TiO_2 calculations; eight **q** points and 1000 levels are used in wurtzite ZnO calculations; and five **q** points and 1000 levels are used in zincblende ZnO calculations. We checked that all these values are needed to obtain convergence of the band energies.

IV. RESULTS

Table I summarizes the band gaps of TiO_2 and ZnO calculated using the LDA and *GW* methods together with the results of the previous *GW* calculations mentioned in Sec. I, and the band structures are shown in Fig. 4. Although the *GW* QP energies are plotted at several **k** points only, we can see that the *GW* and LDA valence bands are similar to each other, while the *GW* and LDA conduction bands are quite different for all these crystals. The band gaps of anatase TiO_2 and rutile TiO_2 are 1.70 and 1.76 eV in the LDA calculation and 3.44 eV (indirect band gap from the *Z* point to the Γ points) and 3.30 eV (indirect band gap from the Γ to the *R* points) in the *GW* calculation, respectively. For wurtzite ZnO and zincblende ZnO, the LDA band gaps are 1.10 and 1.07 eV, and the *GW* band gaps are 2.82 eV (direct band gap at the Γ point) and 2.01 eV (direct at the Γ point), respectively. For wurtzite ZnO, our result of 2.82 eV is comparable to the best (asymptotically fitted) one-shot *GW* band gap of 2.83 eV reported by Friedrich *et al.* [30].

Compared with the experimental data, the LDA results seriously underestimate the band gap. Due to the 3*d* orbitals, there exist local electron correlations in TiO_2 and ZnO. In the LDA calculation, the band structures are not improved by the energy-independent and local exchange correlations. Compared to the LDA results, the self-energy Σ_{xc}^{GW} enlarges the band gap in the *GW* calculation, and the results are close to experimental data also in the case of TiO_2.

Several band gap values of the preexisting *GW* calculations are also listed in Table I. Compared with the one-shot *GW* results, there exists a quite large degree of differences. Our *GW* calculation result for anatase TiO_2 is 3.44 eV, which agrees well with experimental data [2]. In the case of rutile TiO_2, there exist strong local-field effects, and the use of the GPP model overestimates the band gap by about 1 eV ([18]; see also I). Due to the complex structure of the loss function in the rutile TiO_2 crystal, which causes a significant reduction in the dielectric function. These values of the *GW* band gap are very scattered, but our all-electron one-shot *GW* result of

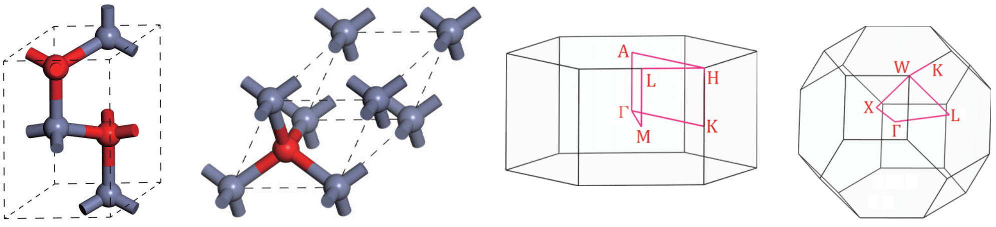

(a)wurtzite ZnO (b)zincblende ZnO (c)1st BZ of wurtzite ZnO (d)1st BZ of zincblende ZnO

FIG. 3. Crystal structure of (a) wurtzite ZnO and (b) zincblende ZnO; first Brillouin zone (BZ) and special **k** points of (c) wurtzite ZnO and (d) zincblende ZnO. Red atoms, oxygen; gray atoms, zinc.

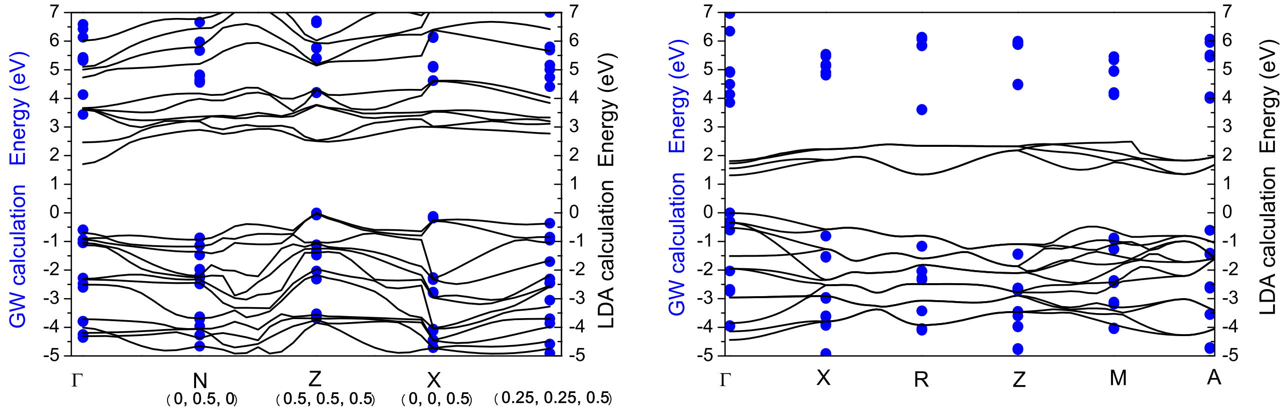

(a)anatase TiO_2 (b)rutile TiO_2

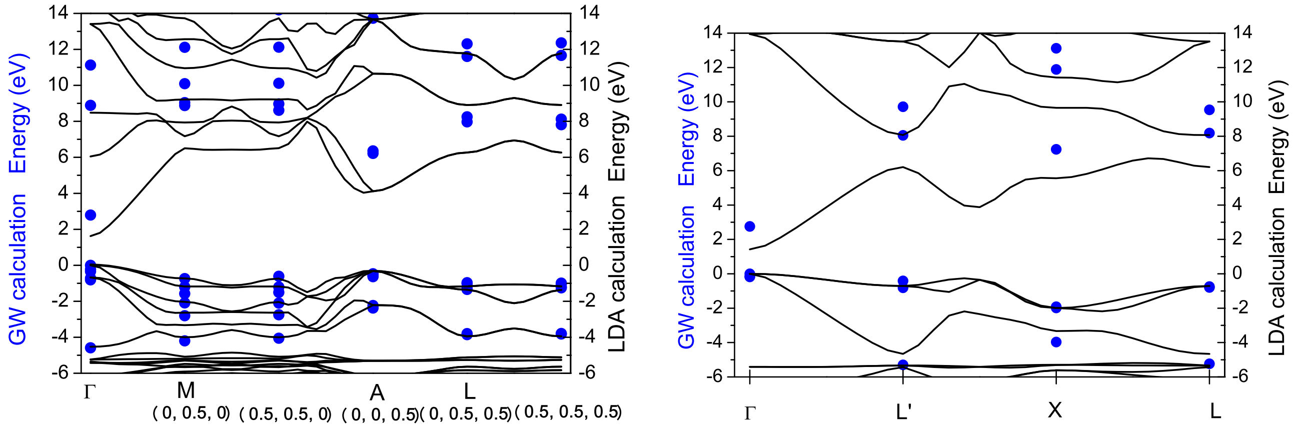

(c)wurtzite ZnO (d)zincblende ZnO

FIG. 4. Band structure of (a) anatase TiO_2, (b) rutile TiO_2 (same as I), (c) wurtzite ZnO, and (d) zincblende ZnO. Lines, the LDA; circles, *GW* calculation. The zero of energy is placed at the top of the valence band (VBM). (α, β, γ) indicates $\mathbf{k} = \alpha\mathbf{b}_1 + \beta\mathbf{b}_2 + \gamma\mathbf{b}_3$, with $\mathbf{b}_1$, $\mathbf{b}_2$, $\mathbf{b}_3$ as the primitive reciprocal lattice vectors.

3.30 eV using the full ω integration is close to the experimental data [3].

There is a significant deviation from the experimental band gap in ZnO systems. The previous one-shot *GW* results are 2.44 eV [26], 2.83 eV [30], 2.352 eV [31], and 2.56 eV [32] for wurtzite ZnO and 2.12 eV for zincblende ZnO [34]. So far, no one has succeeded in obtaining good ZnO results, even using the self-consistent *GW* method and the $GW\Gamma^1$ method. Crüneis *et al.* [33] used the $GW\Gamma^1$ approximation and obtained 3.88 eV for the band gap. Shishkin *et al.* [35] adopted the TC-TC corrections in *W* and obtained 3.2 eV for the band gap. However, these band-gap values do not accord with the experimental data. Our result (2.82 eV for wurtzite ZnO evaluated by ω' integration) is comparable to the previous one-shot *GW* calculations [26,29,31,32]. In practice, Kohn-Sham orbitals and eigenvalues are used as input for a one-shot *GW* calculation. The pseudopotential or the choice of the exchange-correlation functional (including the use of DFT + U) may affect the QP energies in the *GW* calculation. In our calculations, single-electron wave functions are accurately described by PWs and AOs. We set very high cutoff energies for PWs, Fock exchange, and correlations which are capable of describing spatially localized 3*d* states in ZnO systems well. Thus we expect that our all-electron mixed basis calculations give accurate enough QP energies within the one-shot *GW* approximation.

V. DISCUSSION

In the *GW* calculations for anatase TiO_2 and rutile TiO_2, QP energy contributions from the LDA exchange-correlation V_{xc}^{LDA}, the exchange (Σ_x), and the correlation (Σ_c) parts of the self-energy Σ_{xc}^{GW} are listed in Table II. The values of the LDA exchange correlation V_{xc}^{LDA} in the valence band maximum (VBM) and the conduction band minimum (CBM) are very close. The self-energy Σ_{xc}^{GW} values for anatase TiO_2 and rutile TiO_2 are -18.71 and -19.30 eV in the VBM; these values become -15.82 and -17.79 eV in the CBM. The difference $\Sigma_{xc}^{GW} - V_{xc}^{\mathrm{LDA}}$ is larger in the CBM than in the VBM. Consequently, the *GW* method increases the gap between the valence and the conduction states and improves the underestimated LDA results.

Table III lists the QP energy contributions in the *GW* calculations for wurtzite ZnO and zincblende ZnO. The

TABLE II. Contributions to the quasiparticle energies of anatase and rutile TiO_2 at the conduction band minimum (CBM) and valence band maximum (VBM) (in eV).

State	Σ_x	Σ_c	Σ_{xc}^{GW}	V_{xc}^{LDA}	$\varepsilon^{\mathrm{LDA}}$	ε^{GW}
Anatase						
CBM	– 11.98	– 3.84	– 15.82	– 21.23	9.10	12.88
VBM	– 21.43	2.72	– 18.71	– 21.21	7.40	9.44
Rutile						
CBM	– 13.16	– 4.63	– 17.79	– 21.90	10.52	13.78
VBM	– 22.21	2.91	– 19.30	– 21.58	8.76	10.48

LDA results also underestimate the band gap, while the *GW* approximation increases the band gap, producing better results. The value for the exchange part of the self-energy Σ_x of wurtzite ZnO in the CBM is -9.20 eV, and that of zincblende ZnO is -9.38 eV. Compared with Table II, the Σ_x value of anatase TiO_2 and rutile TiO_2 in the CBM are -11.98 and -13.16 eV. The absolute values of Σ_x for ZnO in the CBM are much smaller than that for TiO_2. From Eq. (10), the Σ_x value is estimated with the following equation:

$$\langle\psi_{n\mathbf{k}}|\,\Sigma_x(\mathbf{r},\mathbf{r}')\,|\psi_{n\mathbf{k}}\rangle = -\sum_{n'\mathbf{k}'}^{\mathrm{occ}}\iint\frac{\psi_{n\mathbf{k}}^*(\mathbf{r})\psi_{n'\mathbf{k}'}(\mathbf{r})\psi_{n'\mathbf{k}'}^*(\mathbf{r}')\psi_{n\mathbf{k}}(\mathbf{r}')}{|\mathbf{r}-\mathbf{r}'|}d\mathbf{r}d\mathbf{r}'. \quad (15)$$

Since the summation runs over the occupied states only, if $|\psi_{n\mathbf{k}}\rangle$ is an occupied state, the Σ_x value is a large negative; on the other hand, if $|\psi_{n\mathbf{k}}\rangle$ is an empty state, there is no large overlap between $\psi_{n\mathbf{k}}$ and $\psi_{n'\mathbf{k}'}$, leading to a small negative value of Σ_x. These tendencies are well observed in both Table II and Table III. There is much less overlap of the occupied states of ZnO than of TiO_2, with the unoccupied states in the CBM. This is because the electron configuration is $1s^22s^22p^63s^23p^63d^24s^2$ for Ti atoms and $1s^22s^22p^63s^23p^63d^{10}4s^2$ for Zn atoms, and $3d$ orbitals are fully occupied in Zn atoms but not in Ti atoms.

Similarly, the absolute value for the correlation part of the self-energy Σ_c of ZnO in the CBM is smaller than that of TiO_2, reflecting the fact that the electron screening effect becomes larger as the absolute value of the exchange part Σ_x becomes larger. It is also interesting to note that the values of Σ_c for the VBM, i.e., for the occupied states, are all positive and not small numbers. This indicates again that the electron screening effect to reduce the exchange interaction is strong in these materials.

TABLE III. Contributions to the quasiparticle energies of wurtzite and zincblende ZnO at the conduction band minimum (CBM) and valence band maximum (VBM) (in eV).

State	Σ_x	Σ_c	Σ_{xc}^{GW}	V_{xc}^{LDA}	$\varepsilon^{\mathrm{LDA}}$	ε^{GW}
Wurtzite						
CBM	– 9.20	– 3.07	– 12.27	– 13.27	10.01	11.01
VBM	– 32.07	3.74	– 28.33	– 27.87	8.91	8.19
Zincblende						
CBM	– 9.38	– 2.55	– 11.93	– 14.11	9.14	11.32
VBM	– 28.28	2.21	– 26.07	– 27.32	8.07	9.31

Our LDA band gap of ZnO is a bit larger compared with the preexisting results. In the all-electron mixed basis approach, AOs exceeding the nonoverlapping atomic sphere are modified by subtracting smooth polynomial functions to be confined inside this sphere. The polynomial functions smoothly connecting to the original AOs outside this sphere can be well expressed by PWs. If we remove valence Zn $3d$ valence AOs from the calculations, the resulting LDA energy gap becomes 0. Therefore, the inclusion of Zn $3d$ AOs is essential to obtain a finite energy gap as well as O $2s$ and O $2p$ valence AOs.

Now we focus on the core states in order to discuss the effect of the all-electron mixed basis calculation in the case of the wurtzite ZnO crystal in particular. LDA core-state eigenvalues of an isolated atom without relativistic effect ("isolated atom") and those of a wurtzite ZnO crystal ("$\varepsilon^{\mathrm{LDA}}$") are listed in Table IV, in Hartree atomic units. Also, the values of AO-AO Hamiltonian matrix elements with and without semirelativistic effect are listed in the same table, as well as the semirelativistic effect itself. The values are at the Γ point, although there is no difference even at other $\mathbf{k}$ points. The final eigenvalues $\varepsilon^{\mathrm{LDA}}$ include the PW contributions also. The values in columns 2 and 3 ("Isolated atom" and "$\langle\mathrm{AO}|H|\mathrm{AO}\rangle$"), without relativistic correction, are very close to each other, which means that the spherical part of the potential is similar to that of the isolated atoms. The semirelativistic correction $\langle\mathrm{AO}|R|\mathrm{AO}\rangle$ includes Darwin and mass-velocity terms and is larger in s orbitals than in p orbitals as expected. The difference between $\langle\mathrm{AO}|H+R|\mathrm{AO}\rangle$ and $\varepsilon^{\mathrm{LDA}}$ is mainly due to the PW contributions to the corresponding state. Although the PW contributions may have a large semirelativistic effect for the Zn $1s$ state, these two values are not so very different except for Zn $1s$. The difference becomes larger for Zn $3s$ and $3p$, indicating that a frozen core approximation cannot be used for these orbitals.

In our result, we did not take into account the effect of the off-diagonal elements of the self-energy correction $\langle n\mathbf{k}|\Sigma_{xc}^{GW}-V_{xc}^{\mathrm{DFT}}|n'\mathbf{k}\rangle$, because usually it is ignored in the one-shot GW calculation. We calculated the off-diagonal elements of the self-energy correction, $\langle n\mathbf{k}|\Sigma_{xc}^{GW}-V_{xc}^{\mathrm{DFT}}|n'\mathbf{k}\rangle$. For the $N(N-1)/2(=1770)$ off-diagonal elements with $N=60$, Table V lists the histogram data for the magnitude of the off-diagonal elements. In this table, one can see that the off-diagonal elements of ZnO are slightly larger than those of TiO_2. However, there is no big difference between them. This probably indicates that not only the off-diagonal elements but also the higher-order diagram contributions are important in ZnO crystals.

VI. CONCLUSION

The QP band structure of anatase TiO_2, rutile TiO_2, wurtzite ZnO, and zincblende ZnO were calculated using the all-electron mixed basis one-shot *GW* method with our original full ω-integration technique, which is very efficient and accurate. The LDA gives too small band gaps as usual. In the *GW* calculations, the difference $\Sigma_{xc}^{GW}-V_{xc}^{\mathrm{LDA}}$ evaluated in the CBM becomes larger than that in the VBM, which leads to a large change in quasiparticle energy between the VBM and the CBM. Consequently, the *GW* method enlarges the gap between the valence and the conduction states and

TABLE IV. LDA core-state eigenvalues of an isolated atom without relativistic effect and those of a wurtzite ZnO crystal with semirelativistic effect ($\varepsilon^{\mathrm{LDA}}$) (in Hartree atomic units). Also, the values of AO-AO Hamiltonian matrix elements with and without semirelativistic effect $\langle \mathrm{AO}|R|\mathrm{AO}\rangle$ are listed, respectively, as $\langle \mathrm{AO}|H+R|\mathrm{AO}\rangle$ and $\langle \mathrm{AO}|H|\mathrm{AO}\rangle$.

	Isolated atom	$\langle \mathrm{AO}\|H\|\mathrm{AO}\rangle$	$\langle \mathrm{AO}\|R\|\mathrm{AO}\rangle$	$\langle \mathrm{AO}\|H+R\|\mathrm{AO}\rangle$	$\varepsilon^{\mathrm{LDA}}$
Zn 1s	−344.971	−344.938	−5.137	−350.075	−350.490
Zn 2s	−41.532	−41.542	−1.143	−42.685	−42.747
Zn 2p	−36.649	−36.084	−0.791	−36.875	−36.884
O 1s	−18.759	−17.920	−0.024	−17.944	−17.948
Zn 3s	−4.573	−4.139	−0.310	−4.449	−4.215
Zn 3p	−3.022	−2.279	−0.048	−2.237	−2.525× 4

improves the underestimated LDA results. Thus we found that our method of electronic structure calculation using the all-electron mixed basis one-shot *GW* approximation produces reasonable band-gap results for both the $\mathrm{TiO_2}$ and the ZnO systems, and the agreement with the experimental band gap is excellent especially for $\mathrm{TiO_2}$ systems. We have discussed the core contributions in the LDA level and off-diagonal elements of the self-energy correction in the *GW* level.

TABLE V. Histogram table of the off-diagonal elements $\langle n\mathbf{k}|\Sigma_{xc}^{GW} - V_{xc}^{\mathrm{DFT}}|n'\mathbf{k}\rangle$.

eV	$\mathrm{TiO_2}$ anatase	$\mathrm{TiO_2}$ rutile	ZnO wurtzite	ZnO zincblende
0.0–1.0	1739	1742	1714	1728
1.0–2.0	17	17	41	22
2.0–3.0	11	10	8	9
3.0–4.0	3	0	5	8
4.0–5.0	0	1	1	3
5.0–6.0	0	0	0	0
6.0–7.0	0	0	1	0

In Zn atoms, 3d orbitals are fully occupied by narrow energy bands. In such localized states, the effect of electron correlations becomes generally very important. Therefore, it is difficult to accurately describe the QP wave functions in ZnO systems, which leads to the failure of ZnO calculations. In our method, the QP wave functions are described by PWs and AOs, and we obtained better results than the previous one-shot *GW* calculations in ZnO systems. In order to further improve the results, it would be necessary to perform a fully self-consistent $GW\Gamma$ calculation. Although such a high-level calculation is desirable, the present *GW* method may help us to better understand the electronic structure of transition metal oxides that are not strongly correlated.

ACKNOWLEDGMENTS

The authors thank Dr. Riichi Kuwahara for his implementation of the plasmon pole model. This work was supported by a Grant-in-Aid for Scientific Research B (Grant No. 25289218) from JSPS and also by a Grant-in-Aid for Scientific Research on Innovative Areas (Grant No. 25104713) from MEXT. We are also indebted to the HPCI promoted by MEXT for the use of the SR16000 supercomputer at Hokkaido University and at IMR, Tohoku University (Subject Nos. hp140214, hp150076, and hp150231).

---

[1] S. P. Kowalczyk, F. R. McFeely, L. Ley, V. T. Gritsyna, and D. A. Shirley, Solid State Commun. **23**, 161 (1977).

[2] H. Tang, F. Lévy, H. Berger, and P. E. Schmid, Phys. Rev. B **52**, 7771 (1995).

[3] Y. Tezuka, S. Shin, T. Ishii, T. Ejima, S. Suzuki, and S. Sato, J. Phys. Soc. Jpn. **63**, 347 (1994).

[4] S. Rangan, S. Katalinic, R. Thorpe, R. A. Bartynski, J. Rochford, and E. Galoppini, J. Phys. Chem. C **114**, 1139 (2010).

[5] P. J. Hardman, G. N. Raikar, C. A. Muryn, G. van der Laan, P. L. Wincott, G. Thornton, D. W. Bullett, and P. A. D. M. A. Dale, Phys. Rev. B **49**, 7170 (1994).

[6] S. Tsoi, X. Lu, A. K. Ramdas, H. Alawadhi, M. Grimsditch, M. Cardona, and R. Lauck, Phys. Rev. B **74**, 165203 (2006).

[7] H. Alawadhi, S. Tsoi, X. Lu, A. K. Ramdas, M. Grimsditch, M. Cardona, and R. Lauck, Phys. Rev. B **75**, 205207 (2007).

[8] S. F. Chichibu, T. Sota, G. Cantwell, D. B. Eason, and C. W. Litton, J. Appl. Phys. **93**, 756 (2003).

[9] C. Kittel, *Introduction to Solid State Physics*, 6th ed. (Wiley, New York, 1986).

[10] A. Mang, K. Reimann, and S. Rbenacke, Solid State Commun. **94**, 251 (1995).

[11] P. Hohenberg and W. Kohn, Phys. Rev. **136**, B864 (1964).

[12] L. Hedin, Phys. Rev. **139**, A796 (1965).

[13] L. Hedin and S. Lundqvist, *Solid State Physics*, Vol. 23 (Academic Press, New York, 1969).

[14] M. S. Hybertsen and S. G. Louie, Phys. Rev. Lett. **55**, 1418 (1985).

[15] M. S. Hybertsen and S. G. Louie, Phys. Rev. B **34**, 5390 (1986).

[16] R. W. Godby, M. Schlüter, and L. J. Sham, Phys. Rev. Lett. **56**, 2415 (1986).

[17] R. W. Godby, M. Schlüter, and L. J. Sham, Phys. Rev. B **37**, 10159 (1988).

[18] W. Kang and M. S. Hybertsen, Phys. Rev. B **82**, 085203 (2010).

[19] C. E. Patrick and F. Giustino, J. Phys. Condens. Matter **24**, 202201 (2012).

[20] M. Oshikiri, M. Boero, F. A. J. Ye, and G. Kido, Thin Solid Films **445**, 168 (2003).

[21] L. Chiodo, J. M. Garcia-Lastra, A. Iacomino, S. Ossicini, J. Zhao, H. Petek, and A. Rubio, Phys. Rev. B **82**, 045207 (2010).

[22] M. Zhang, S. Ono, and K. Ohno, Phys. Rev. B **92**, 035205 (2015).

[23] M. van Schilfgaarde, T. Kotani, and S. Faleev, Phys. Rev. Lett. **96**, 226402 (2006).

[24] T. Kotani, M. van Schilfgaarde, S. V. Faleev, and A. Chantis, J. Phys. Condens. Matter **19**, 365236 (2007).

[25] S. Lany, Phys. Rev. B **87**, 085112 (2013).

[26] M. Usuda, N. Hamada, T. Kotani, and M. van Schilfgaarde, Phys. Rev. B **66**, 125101 (2002).

[27] S. Massidda, R. Resta, M. Posternak, and A. Baldereschi, Phys. Rev. B **52**, R16977(R) (1995).

[28] B.-C. Shih, Y. Xue, P. Zhang, M. L. Cohen, and S. G. Louie, Phys. Rev. Lett. **105**, 146401 (2010).

[29] C. Friedrich, M. C. Müller, and S. Blügel, Phys. Rev. B **83**, 081101 (2011).

[30] C. Friedrich, M. C. Müller, and S. Blügel, Phys. Rev. B **84**, 039906 (2011).

[31] M. Stankovski, G. Antonius, D. Waroquiers, A. Miglio, H. Dixit, K. Sankaran, M. Giantomassi, X. Gonze, M. Côté, and G.-M. Rignanese, Phys. Rev. B **84**, 241201 (2011).

[32] J. A. Berger, L. Reining, and F. Sottile, Phys. Rev. B **85**, 085126 (2012).

[33] A. Grüneis, G. Kresse, Y. Hinuma, and F. Oba, Phys. Rev. Lett. **112**, 096401 (2014).

[34] M. Shishkin and G. Kresse, Phys. Rev. B **75**, 235102 (2007).

[35] M. Shishkin, M. Marsman, and G. Kresse, Phys. Rev. Lett. **99**, 246403 (2007).

[36] R. Kuwahara and K. Ohno, Phys. Rev. A **90**, 032506 (2014).

[37] M. Rohlfing and S. G. Louie, Phys. Rev. B **62**, 4927 (2000).

[38] G. Onida, L. Reining, and A. Rubio, Rev. Mod. Phys. **74**, 601 (2002).

[39] W. von der Linden and P. Horsch, Phys. Rev. B **37**, 8351 (1988).

[40] J. P. Perdew and A. Zunger, Phys. Rev. B **23**, 5048 (1981).

[41] K. Ohno, K. Esfarjani, and Y. Kawazoe, *Computational Materials Science: From Ab Initio to Monte Carlo Methods* (Springer-Verlag, Berlin, 1999), p. 113, Vol. 129, Fig. 2.23.

[42] R. W. Godby, M. Schlüter, and L. J. Sham, Phys. Rev. B **35**, 4170 (1987).

[43] R. W. Godby, M. Schlüter, and L. J. Sham, Phys. Rev. B **36**, 6497 (1987).

[44] S. Ishii and K. Ohno (unpublished).

[45] K. Ohno, S. Ono, R. Kuwahara, Y. Noguchi, R. Sahara, Y. Kawazoe, and M. H. F. Sluiter, TOMBO Group, http://www.ohno.ynu.ac.jp/tombo/index.html.

[46] S. Ono, Y. Noguchi, R. Sahara, Y. Kawazoe, and K. Ohno, Comput. Phys. Comm. **189**, 20 (2015).

[47] K. Ohno, F. Mauri, and S. G. Louie, Phys. Rev. B **56**, 1009 (1997).

[48] S. Ishii, K. Ohno, Y. Kawazoe, and S. G. Louie, Phys. Rev. B **63**, 155104 (2001).

[49] Y. Noguchi, S. Ishii, and K. Ohno, J. Chem. Phys. **125**, 114108 (2006).

[50] E. Kikuchi, S. Iwata, S. Ishii, and K. Ohno, Phys. Rev. B **76**, 075325 (2007).

[51] S. Ishii, S. Iwata, and K. Ohno, Mater. Trans. **51**, 2150 (2010).

[52] J. K. Burdett, T. Hughbanks, G. J. Miller, J. W. Richardson, Jr., and J. V. Smith, J. Am. Chem. Soc. **109**, 3639 (1987).

[53] S. C. Abrahams and J. L. Bernstein, J. Chem. Phys. **55**, 3206 (1971).

[54] O. Madelung, M. Schulz, and H. Weiss, *Numerical Data and Functional Relationships in Science and Technology* (Springer-Verlag, Berlin, 1982), Vol. 17.

[55] M. Oshikiri and F. Aryasetiawan, Phys. Rev. B **60**, 10754 (1999).